# ZnO Nanobelt Arrays Grown Directly from and on Zinc Substrates: Synthesis, Characterization, and Applications

**Xiaogang Wen,[†] Yueping Fang,[†] Qi Pang,[†] Chunlei Yang,[‡] Jiannong Wang,[‡] Weikun Ge,[‡] Kam Sing Wong,[‡] and Shihe Yang*,[†]**

*Department of Chemistry, Institute of Nano Science and Technology, The Hong Kong University of Science and Technology, Clear Water Bay, Kowloon, Hong Kong, China, and Department of Physics, The Hong Kong University of Science and Technology, Clear Water Bay, Kowloon, Hong Kong, China*

*Received: May 11, 2005; In Final Form: June 11, 2005*

In situ growth of ZnO nanobelt arrays from and on zinc substrates (foils and microparticles) has been accomplished by controlled thermal oxidation in the presence of oxygen. The nanobelts grow approximately perpendicular to the Zn substrate surface along the $\langle 11\bar{2}0\rangle$ direction of ZnO, which has a thickness of ∼3−4 nm, a width tapering from about 50 to 300 nm, and a length of ∼10−20 $\mu$m. On the basis of the structural analysis and kinetic studies, a tip-growth mechanism is proposed, which underlines the transport of Zn from the substrate to the growing tip. The ratio of UV to green photoluminescent emissions of the as-synthesized ZnO nanobelt arrays could be controlled by varying the reaction conditions. Sharp UV stimulated emission peak is also observed at moderate threshold excitation intensity (∼0.7 mJ/cm$^2$) showing the high quality of the ZnO nanobelts. The ZnO nanobelts array has also been tested for sensing $NH_3$ gas, and high sensitivity, reversibility, and rapid response have been demonstrated.

## Introduction

ZnO is a remarkable semiconductor with a wide band gap of 3.37 eV and a large exciton binding energy of 60 meV. Shrinking this material to one dimension (1D) is expected to open wide-ranging application possibilities from room-temperature ultraviolet (UV) lasers,[1−4] sensors,[5−11] photocatalysts,[12] solar cells,[13,14] to field-emission (FE) devices.[15] Recently, a gamut of methods, including vapor−liquid−solid (VLS), vapor−solid (VS), hydrothermal, and other solution processes have been used to produce all kinds of 1D ZnO entities ranging from nanowires,[16−19] nanobelts,[20−23] nanorods,[24−30] nanotubes,[31,32] nanoneedles,[15] to hierarchical nanostructures.[33−36] Moreover, well-aligned ZnO nanowire or nanorod arrays have also been fabricated on a variety of substrates, which are important for device applications. The techniques used for growing ZnO nanowire or nanorod arrays mainly include template,[18] patterned catalytic growth,[16,17,24] substrate-induced vapor deposition,[23,25,26,34,37] and solution-phase deposition.[27,28,31] These methods often confront problems of templates/catalyst removal, tedious operation procedures, poor adhesion of nanowires to the underlying substrate, etc.

An alternative strategy is to grow nanowire or nanobelt arrays directly from metal substrates so that the nanowire synthesis and assembly are accomplished in one step without templates. This method has the virtue of simplicity, efficiency, and low cost, which facilitates device fabrication and characterizations. In principle, patterned nanowire arrays created using this method can be electrically addressed by the supporting substrate electrodes. The feasibility in realizing the above strategy is largely assured by the omnipresent crystal growth anisotropy, the asymmetry at the substrate surface, and the mutual support and exclusion of the vertically grown nanowires. By exploitation of this concept, we have successfully synthesized 1D nanomaterial arrays, including $Cu_2S$,[38] $Cu(OH)_2$,[39,40] CuO,[41] and $Fe_2O_3$,[42] on metal substrates using both gas−solid and solution−solid reactions. Consequently, this has allowed us to scrutinize FE and transport properties of these intriguing arrays of materials. In the present work, we grow well-aligned ZnO nanobelt arrays directly on Zn substrates by thermal oxidation in the atmosphere of oxygen. The photoluminescence, stimulated emission, and ammonia sensing properties of the as-synthesized ZnO nanobelt arrays are studied.

## Experimental Section

The experimental setup consists of a horizontal tube furnace (5 cm × 40 cm) and a quartz tube (4.5 cm × 60 cm). Zinc foils (10 mm × 10 mm × 0.2 mm) with a purity of 99.9% and zinc particle powders with a purity of 98% (diameter = ∼4−10 $\mu$m) were purchased from Aldrich. The Zn foils were carefully cleaned with absolute ethanol three times and loaded onto a ceramic substrate. For Zn microparticles, the sample was dispersed in ethanol in an ultrasonic bath for 30 min and the resultant suspension was rapidly dropped onto a silicon or quartz substrate. After evaporation of ethanol in air, the substrate coated with the Zn microparticles was loaded into a quartz boat. The quartz boat or ceramic substrate was positioned in the middle of the quartz tube and also the middle of the tube furnace. The tube furnace was heated at a rate of 20 °C/min to a designated temperature. After being held at this temperature for an appropriate time, the system was cooled naturally to room temperature. A white product layer was found to be homogeneously coated on the substrate.

The as-prepared ZnO products on the substrate were directly subjected to characterizations by scanning electron microscopy (SEM) and powder-X-ray diffraction (XRD). For transmission electron microscopy (TEM) observations, the ZnO nanobelts

* To whom correspondence should be addressed. E-mail: chsyang@ust.hk.
[†] Department of Chemistry, Institute of Nano Science and Technology.
[‡] Department of Physics.

10.1021/jp052466f CCC: $30.25 
Published on Web 07/23/2005

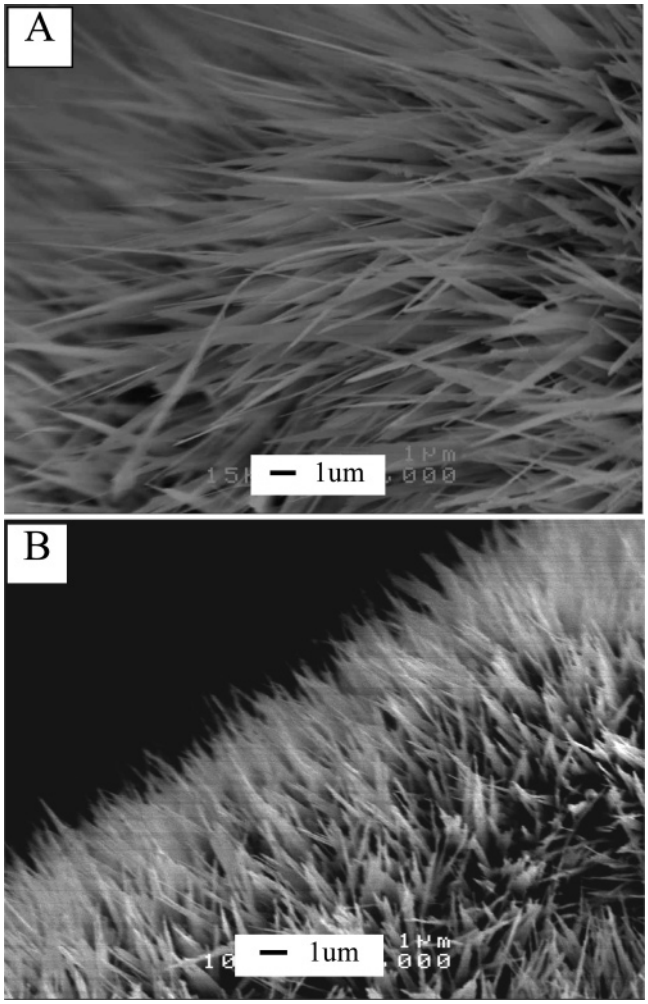


**Figure 1.** Typical SEM images of a ZnO nanobelts array grown (at 600 °C for ~6 h) on a Zn foil. (A) Top view. (B) Side view.

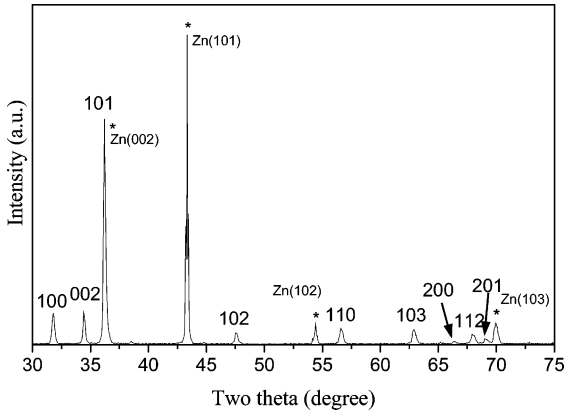


**Figure 2.** XRD pattern of a ZnO nanobelts array synthesized on a Zn foil (at 600 °C for 6 h).

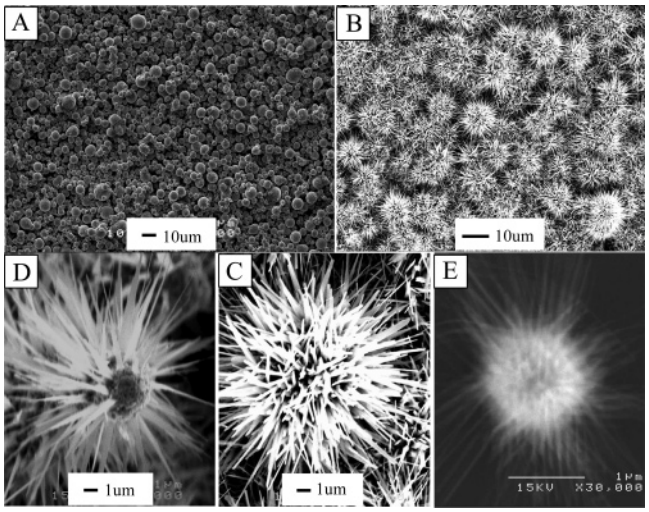


**Figure 3.** SEM images of ZnO nanobelts grown from Zn microparticles. (A) Zn microparticles cast on a p-type low-resistance Si wafer before the growth of ZnO nanobelts; (B) ZnO nanobelt balls grown from and on the Zn microparticles; (C) a single ball with densely packed ZnO nanobelts; (D) a single ball with a region of sparse nanobelts; (E) a single ZnO nanobelt ball grown from a smaller core.

were transferred onto carbon-coated copper grids by gently sliding the Cu grid on the surface of the sample. The XRD analysis was performed on a Philips PW-1830 X-ray diffractometer with Cu Kα irradiation ($\lambda = 1.5406$) at a scanning speed of 0.025 °/s over the $2\theta$ range of 30−75°. The morphologies and elemental compositions of the nanobelts were characterized using SEM (JEOL 6300 and JEOL 6300F) at an accelerating voltage of 15 kV. TEM observation was carried out on Philips CM20 and JEOL 2010F microscopes operated at 200 kV. Photoluminescence (PL) was measured using the He−Cd laser (325 nm) as the excitation source by a spex 500M spectrometer equipped with a photomultiplier tube. For stimulated emission measurement, the sample was excited by a pulsed frequency tripled Nd:YAG laser ($\lambda = 355$ nm, 70-ps pulse width, and 10-Hz repetition rate). A cylindrical lens was used to focus the laser into a rectangular strip of area ~1 mm × 0.2 mm for strip excitation, and the emission was collected from the sample edge and detected by a spectrometer coupled to a charge-coupled device. To measure sensor response to gases, a homemade sensor chamber was used for gas manipulation and control and the current−voltage characteristics were measured using a Keithley 236 source measure unit.

## Results and Discussion

**Synthesis and Structural Characterizations.** Figure 1 shows typical SEM images of the as-grown ZnO nanobelts on the Zn foil. Even at a relatively low temperature (600 °C), ZnO nanobelts could be grown effectively on the Zn substrate. From the top view (A), a beltlike morphology is apparent. These nanobelts are 100−300 nm in width at the root, 10−20 $\mu$m in length, and only about 3−4 nm in thickness (see TEM image in Figure 5B). Most of the nanobelts do not have a uniform width; they become thinner from the root to the top end and form a sharp edge at the tip. The coverage of the ZnO nanobelt array on the substrate appears to be quite uniform with an aerial density of about $10^{14}$ nanobelts/m$^2$. Furthermore, from the cross-sectional view (Figure 5B), the ZnO nanobelts are aligned in a dense array that is approximately perpendicular to the substrate surface. The ZnO nanobelt phase was determined by the XRD pattern in Figure 2, which was recorded directly on an as-prepared array on a substrate. Clearly, all the peaks are in conformity with zincite ZnO ($a = 3.2498$ Å, $c = 5.2066$ Å; calculated values based on the XRD data are $a = b = 3.252$ Å, $c = 5.203$ Å) except the signal of Zn metal from the substrate.

Reaction temperature is a critical parameter for the growth of the ZnO nanobelts (see Figure S1A in Supporting Information). At 400 °C, only sparse and short nanobelts are formed. A raise in the temperature to 550 °C results in the formation of lots of nanobelts on the substrate. At an even higher temperature (e.g., 600 °C), dense and long nanobelt arrays take shape; also the nanobelts become a little wider at higher temperatures.

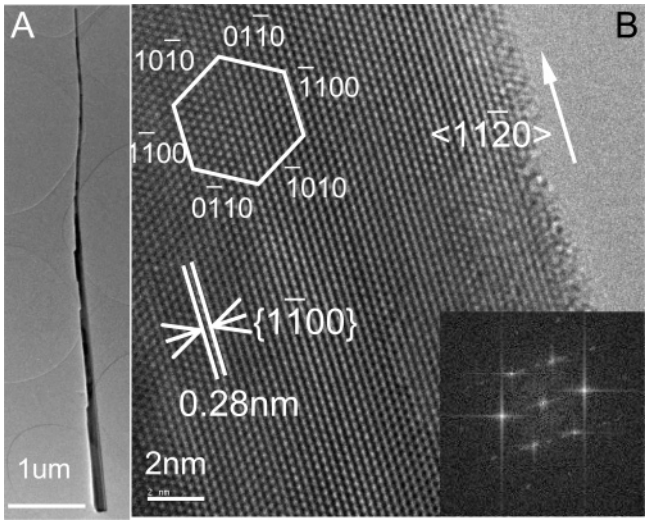


**Figure 4.** (A) TEM image of a single ZnO nanobelt; (B) HRTEM image of a single ZnO nanobelt together with the corresponding FFT pattern (inset). The nanobelt was grown on Zn foil.

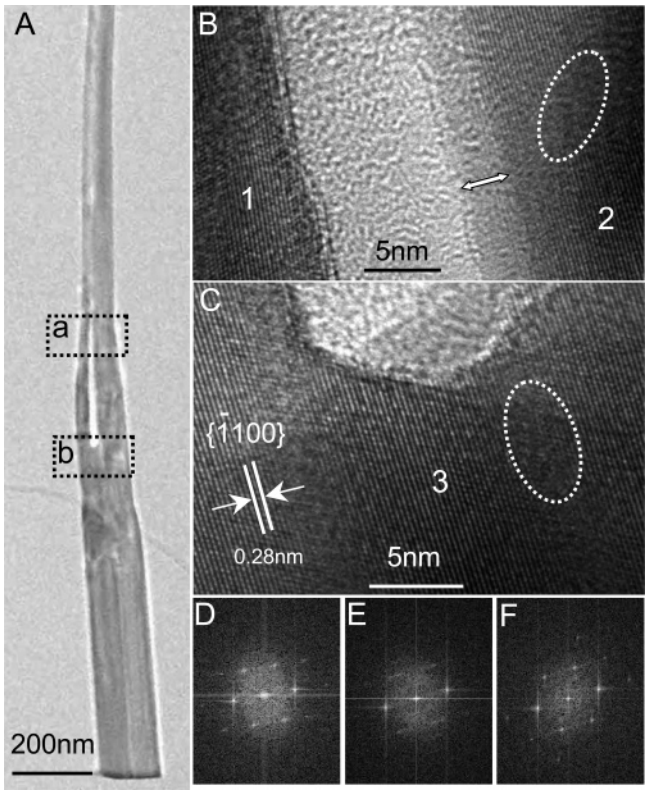


**Figure 5.** (A) TEM image of a single ZnO nanobelt bifurcated into two branches toward the narrow end; (B and C) expanded view of the areas enclosed by the black dashed rectangles (a and b) in (A); (D, E, and F) corresponding FFT patterns recorded from the areas labeled as 1, 2, and 3 in (B) and (C). The nanobelt was grown on Zn foil.

Although ZnO nanobelts can grow on Zn foils as described above, the Zn foils are usually roughened and distorted when the growth temperature (500−600 °C) is above the melting point (420 °C) (see also Figure S1D in Supporting Information). As a result, well-aligned ZnO nanobelt arrays could be grown only at some local areas.

To create a large-area, uniform array of ZnO nanobelts on a substrate for device applications, a film of micrometer-sized Zn particles is used to replace the Zn foil as the growth substrate. The Zn microparticles can be easily coated on different substrates such as quartz, silicon, indium−tin oxide (ITO), etc., which can be selected depending on specific applications. Because the nanobelts are grown on individual Zn microparticles, growth-induced stresses often encountered on Zn foils are avoided here so that uniform nanobelt films can be fabricated in large areas. In addition, the hierarchical nanobelt ball structure of ZnO in the form of a film provides new opportunities for device design and applications. For example, a ZnO microparticle coated with radial nanowires or nanobelts may serve as a light harvest antenna as well as a micro-laser source.

The SEM images in Figure 3 illustrate how ZnO nanobelts are radially grown from Zn microparticles cast as a film. Here the Zn microparticles (mostly 4−10 $\mu$m in diameter) were uniformly coated on a Si wafer. First, the Si wafer was washed with ethanol at least three times. The Zn microparticles were dispersed in an ethanol solution in an ultrasonic bath for 30 min. The ethanol suspension of the Zn microparticles was then dropped onto the washed Si wafer to form a thin film. After drying in air, the Zn microparticle film was uniform (Figure 3A) and used to grow ZnO nanobelts. At a growth temperature of 600 °C, ZnO nanobelts can indeed grow from the Zn microparticles directly to form a dense layer (Figure 3B) and the Zn microparticles are effectively transformed into ZnO nanobelt microballs. From the higher magnification SEM image in Figure 3C, the nanobelts are well-aligned on the microparticle surface, forming a radiating nanobelt spherical shell like a sea urchin. The lengths of the nanobelts are uniform (6−10 $\mu$m) but in general shorter than those grown from Zn foil substrates (10−20 $\mu$m) owing to a more limited supply of Zn from the microparticles. XRD analysis indicates that the Zn microparticles have been completely transformed to ZnO in contrast to the case using Zn foils, where unconverted Zn still exists after reaction. Close inspection of sparse regions of the ZnO nanobelt-decorated balls (Figure 3D) reveals that the core is also ball-like and consists of ZnO according to the XRD and EDX analyses. The core is likely to be porous because its content has been used to sustain the ZnO nanobelt shell. Note that these nanobelts also have a sharp tip; they have a width of 100−300 nm at the roots and 5−10 nm at the tip. The thickness of the nanobelts is believed to be only several nanometers, which has been estimated for the nanobelt grown on Zn foil (Figure 5B). Another note is that the Zn microparticle size has an obvious effect on the width of the ZnO nanobelts grown on the nanoparticle surface. With a Zn core about 1 $\mu$m in diameter, the grown ZnO nanobelts have a width of 20−30 nm and a length of ~1−2 $\mu$m (Figure 3E), which are, respectively, about an order of magnitude smaller than those of the nanobelts grown from the ~5 $\mu$m Zn microparticles (Figure 3D). This demonstrates that the size and even the morphology of the ZnO nanobelts can be controlled by adjusting the amount of Zn source, which is essentially the size of the Zn microparticle.

Shown in Figure 4 are TEM images of a single ZnO nanobelt. Clearly, the nanobelt has a needle shape with a width of 150 nm at the root and 20 nm at the tip (Figure 4A). Consequently, the side surfaces of the nanobelt are not very smooth and steps tend to form along its axial direction. The high-resolution TEM (HRTEM) image (Figure 4B) exhibits clear fringes parallel and perpendicular to the nanobelt axis with fringe spacings of 0.28 and 0.16 nm, which are in good agreement with the interplanar spacings of {1$\bar{1}$00} and {11$\bar{2}$0}, respectively. The single crystalline nature of the ZnO nanobelt can be appreciated from the fast Fourier transform (FFT) pattern in the bottom right inset of Figure 4B. The white hexagon in the top left inset of Figure 4B shows the six relevant crystal planes of the ZnO nanobelt based on the observed fringes along the three directions. Taken

together, it can be concluded that the ZnO nanobelts grow along the $\langle 11\bar{2}0\rangle$ direction and closed by the ($\pm$0001) planes on the top and bottom sides. This result is very different from most of the ZnO 1D nanostructures synthesized using other methods, in which ZnO often grow along the [0001] direction. One exception was reported by Wang's group,[21] who found the growth of ZnO nanobelts to be along $[01\bar{1}0]$ besides [0001] when Sn was used as a catalyst. This was attributed to the fact that the ZnO $(01\bar{1}0)$ crystal face matches well that of Sn (200). Obviously, a different growth mechanism is involved with our method. The key difference with our method is that we use a gas−solid reaction, in which a tip-growth mechanism is probably operative. In essence, the Zn atoms have to undergo solid-phase diffusion through the nanobelt to the tip to maintain the growth. As a result, the growth direction is likely dictated by the balance between the growth rate and the diffusion rate of Zn atoms along a given direction, and this makes the $[11\bar{2}0]$ axis a preferential growth direction of the ZnO nanobelts. Note that the alternate atomic layers in the (0001) planes may be particularly suitable for the transport of Zn atoms from the roots to the tips of the ZnO nanobelts because each layer consists of a single type of atoms. This is also the case for the growth of $\alpha$-$Fe_2O_3$ nanobelts.[42]

Some branched ZnO nanobelts are frequently found in the as-synthesized products. A typical example is given in Figure 5. It is seen that the ZnO nanobelt bifurcates into two branches in the middle (Figure 5A). Such a bifurcation is likely caused by the presence of surface poisons or defects, which may terminate the nanobelt growth at the locations of occurrence. HRTEM images on both branches show the same fringes parallel to the nanobelt axis with a fringe spacing of 0.28 nm (parts B and C of Figure 5), which conforms with the interplanar spacing of $\{\bar{1}100\}$ of ZnO. This shows that both of the ramified branches from the trunk have the same crystal structure and grow along the same direction of $\langle 11\bar{2}0\rangle$. A clear step can be seen on the right branch in Figure 5B (indicated by a white double-headed arrow), which indicates a thickness of about ~3−4 nm for the ZnO nanobelt. Crystal defects can also be spotted in parts B and C of Figure 5 (labeled by white dashed ellipsoids), which may arise from the Zn atom diffusion during growth. The FFT patterns recorded in the regions of the trunk and the two branches show a similar spot pattern (parts D, E, and F of Figure 5) except that the pattern in Figure 5D is slightly distorted due to a small deflection of the left branch as can be seen in Figure 5A. This confirms that different regions of the nanobelt have the same crystal structure with a similar orientation.

It should be pointed out that the bifurcated growth described above strongly supports the tip-growth mechanism of the ZnO nanobelts. We notice that the bifurcation occurs toward the narrow end of the nanobelt. If the growth site is at the root, two independent nanobelts in a distance would have to grow at the same time, at same rate, and with the same orientation and finally merge together seamlessly. This is an unlikely scenario. On the other hand, the tip-growth mechanism is more plausible because the growth sites at the tip could be blocked during reaction so that growth could be terminated at certain points, leading to the formation of ~5−10% branched nanobelts. As mentioned above, the Zn atom diffusion is essential to the growth of the ZnO nanobelts. This is why the growth direction of $[11\bar{2}0]$ is selected because the diffusion in the Zn layers (0001) is likely to be most facile. Such a tip-growth mechanism is also consistent with the fact that the ZnO nanobelts become narrower when they grow longer from the root to the tip. Here the Zn atom diffusion appears to be the limiting factor, and the growing tip of a longer nanobelt is expected to have a more restricted supply of Zn so that a needle shape will be developed as observed.

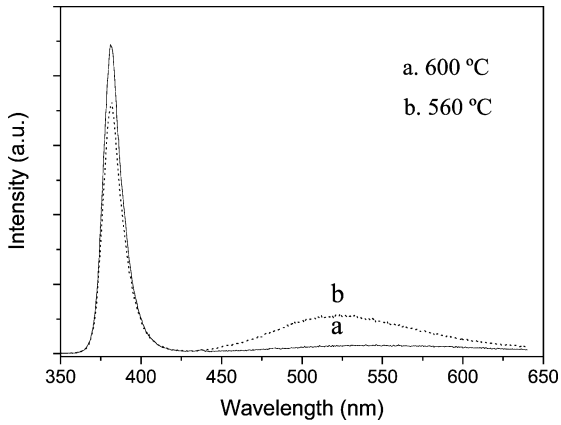


**Figure 6.** Room-temperature PL spectra of ZnO nanobelts arrays synthesized at 560 °C (dotted line) and 600 °C (solid line). The reaction time was ~6 h.

Two most recent reports came to our attention, which are closely related to the present work. One is the synthesis of ZnO nanobelts by a low-temperature evaporation route of metallic Zn plates,[43] and the other is the growth of two-dimensional dendritic ZnO nanowires from oxidation of Zn microcrystals.[44] Although these experiments are similar to ours in one way or another, the reaction conditions (temperature, pressure, gas flow, etc.) and the 1D morphology of ZnO are quite different. For example, the nanobelts in ref 43 mostly grow along the [0001] direction, whereas ours grow along the $[11\bar{2}0]$ direction, which rather agrees with the result in ref 44. However, the nanowires in ref 44 grow in a dendritic fashion, which is also different from our case. In addition, the ZnO nanobelts we prepared have a characteristic needle structure, which contrasts markedly with those of the nanowires in both refs 43 and 44. Most importantly, our systematic studies have established a tip-growth and through-wire transport mechanism for the ZnO nanobelts described above. Optical and gas-sensing properties of these unique ZnO nanobelts have also been studied, which will be presented below.

**Optical and Gas-Sensing Properties.** The new ZnO nanobelts we have synthesized provide opportunities for investigating their optical and gas-sensing properties. First, room-temperature PL has been measured for nanobelts synthesized at different temperatures with excitation at 325 nm. The result is shown in Figure 6. For the sample prepared at 600 °C, only a strong UV emission at 381 nm is observed, which is from the near band edge emission of ZnO. However, PL of nanobelts synthesized at 550 °C displays a weaker UV emission at 381 nm accompanied by a broad green emission band (450−600 nm). It has been suggested that the green band emission correspond to singly ionized oxygen vacancies in ZnO.[45] It is understandable that more defects such as oxygen vacancies are created at lower temperature. As temperature increases, there is enough energy to annihilate the defects that the green emission band is eliminated. This demonstrates that the quality of the ZnO nanobelts we synthesized at higher temperature is very good.

We have also studied stimulated emission properties of the ZnO nanobelts arrays. In this case, the sample was excited by a 70-ps pulsed laser ($\lambda$ = 355 nm). Figure 7A shows emission intensity of the ZnO nanobelts on silicon and glass substrate as a function of excitation intensity; it indicates that all ZnO nanobelts samples show amplified spontaneous emission, i.e.,

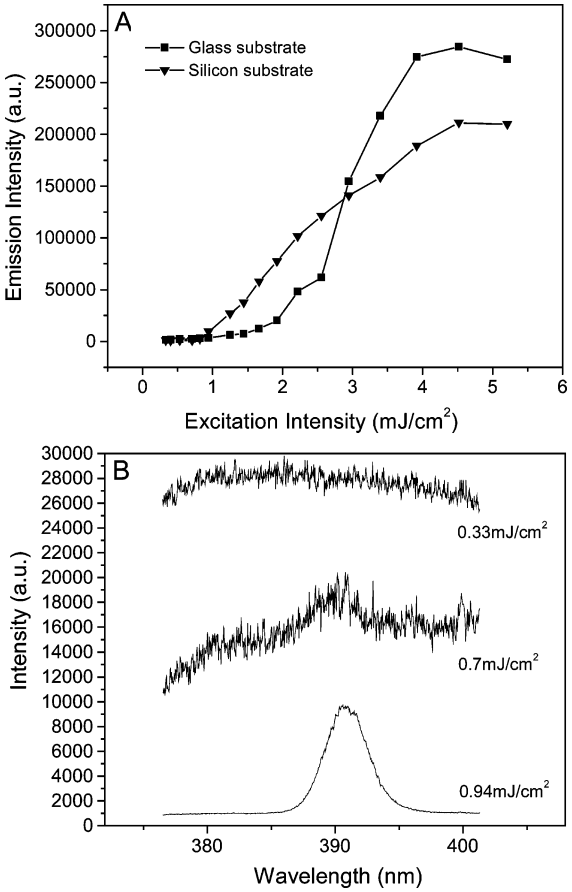


**Figure 7.** (A) Emission intensities of the ZnO nanobelts on silicon and glass substrates as a function of excitation intensity; (B) emission spectra of the ZnO nanobelts on silicon substrates as a function of excitation intensity.

spontaneously emitted photons amplified by stimulated emission. The excitation thresholds for stimulated emission are approximately 0.7 and 1.0 mJ/cm$^2$ for the ZnO nanobelts array on silicon and glass, respectively. The superlinear increase in stimulated emission intensity near threshold is clearly evidenced. And the stimulated emission threshold value of 0.7 mJ/cm$^2$ (silicon substrate case) is several times smaller than those with similar ZnO nanostructures reported recently.[46−48] Shown in Figure 7B are emission spectra of the ZnO nanobelts on silicon substrate as a function of excitation intensity, in which dramatic narrowing of the emission spectrum near 390 nm is demonstrated for excitation above the threshold (∼0.7 mJ/cm$^2$).

As an n-type semiconductor, ZnO has been extensively used as a $NH_3$-sensing material. Up to now, most of these studies have focused on ZnO thin film at high temperatures.[8−10] A notable exception is the work by Rao et al., who studied $NH_3$ sensitivity of ZnO-based film sensor consisting of powder ZnO and other doping components (Fe, Ru, Pd, etc.) at room temperature (30 °C).[11] No measurements of ZnO nanowire sensor responses to $NH_3$ have been reported until now. By consideration that our ZnO nanobelts array should exhibit better sensing performances due simply to the higher surface area, we set out to measure the $NH_3$ sensing characteristics. The ZnO nanobelt sensor configuration is shown in Chart 1, which consists of a low-resistance Si as one of the electrodes and an ITO slide as another electrode pressed on the ZnO nanobelt array. To improve the contact between the ZnO nanobelts and the ITO electrode, a thin soft indium film was formed on the ITO and the current of the sample was measured with a Keithley 236 source measure unit. Figure 8 shows the current response

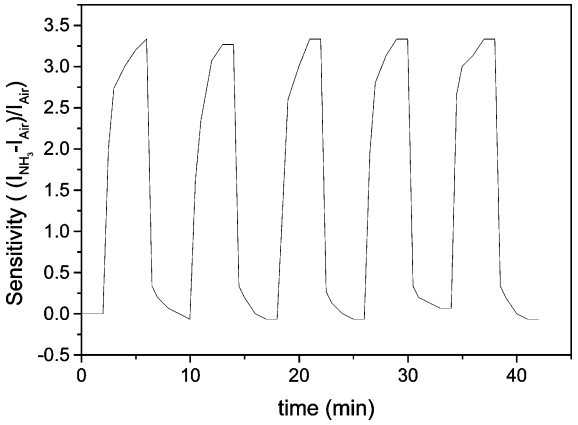


**Figure 8.** Current responses of the ZnO nanobelts sensors when the surrounding gas is switched between air and 500 ppm $NH_3$.

**CHART 1: Schematic Showing the Configuration of the ZnO Nanobelts Sensor**

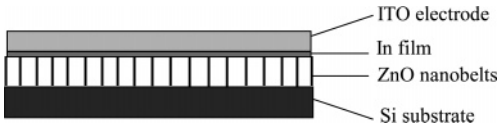


of the sensor to $NH_3$ at room temperature at a bias voltage of 5 V. The sensor is very sensitive to ammonia: when the sensor was exposed to 500 ppm $NH_3$, a current change as high as about 3.5-fold between the on and off states was observed, and this current response to $NH_3$ could be repeated many times without obvious change in signal intensity. The time for the current response to reach 80% of its highest value is about 2 min after adding $NH_3$ and that for it to reach 80% of its lowest value is about 30 s after removing $NH_3$. The repeatability and stability of the sensor appear to be very good. Taken together, our results indicate that the ZnO nanobelt arrays grown from Zn substrate (Zn microparticles) show both high sensitivity and reversibility at the room temperature (25 °C).

For $NH_3$ sensors with ZnO, the change in current is mainly caused by the adsorption and desorption of $NH_3$ and $H_2O$ molecules on the surface of the sensing materials. The high surface-to-volume ratio of our ZnO nanobelts sensor gives rise to high sensitivity to $NH_3$. In addition, the molecules are easy to adsorb on and desorb from the surface of nanobelts in contrast to the conventional thin-film sensor. Note that the exposed surfaces of our ZnO nanobelts are (0001) for the most part, whereas a polycrystalline ZnO film exposes many different crystal planes on the surface, and this may contribute to different sensing properties. For conventional thin-film sensors, an elevated temperature is often used to facilitate molecular desorption. In our nanobelts sensor, however, the available interbelt spaces allow the adsorded molecules to desorb easily in the off state so that it shows a rapid response and good reversibility.

## Conclusions

We have successfully synthesized vertically aligned ZnO nanobelt arrays from and on zinc substrates (both foils and microparticles) by a simple gas−solid reaction process. The ZnO nanobelts are only 3−4 nm in thickness and 10−20 $\mu$m in length, and the width is continually reduced from 50 to 300 nm at the root to 5−10 nm at the tip, resulting in a needle shape. The effects of temperature and microparticle size on the nanobelt growth have been studied, which provide a robust basis for the control of the morphology and size of the 1D nanostructures.

Quite different from the usual VLS growth, our ZnO nanobelts are found to grow following a gas−solid tip-growth mechanism, in which the atomic diffusion in the solid is a rate-determining factor. Moreover, the nanobelts grow along the [11$\bar{2}$0] direction, which is again completely different from the common growth direction of [0001] observed in most of the syntheses of 1D ZnO nanostructures. The advantages of our method include the simplicity, the direct formation of aligned nanobelt films, the ability to control the nanobelt morphology, and the nanobelt growth along a unique crystal direction. PL measurements reveals that the ZnO nanobelts synthesized at lower temperatures contain some defects, but those obtained at higher temperatures possess negligible defects so that only band-gap emission is observed. Sharp UV stimulated emission peak is also observed at moderate threshold excitation intensity ($\sim$0.7 mJ/cm$^2$) showing the high quality of the ZnO nanobelts. The ammonia gas sensor fabricated from the as-synthesized ZnO nanobelt ball arrays on Si substrates shows a high sensitivity and rapid response at room temperature.

**Acknowledgment.** We are grateful to the Research Grant Council of Hong Kong and the Chemistry Department of the Hong Kong University of Science and Technology for supporting the research. S.Y. wishes to thank the Hong Kong Young Scholar Cooperation Research Foundation of NSFC.

**Supporting Information Available:** Figure showing SEM images of ZnO nanobelts grown from Zn foils at different temperatures. This material is available free of charge via the Internet at http://pubs.acs.org.

## References and Notes

(1) Cao, H.; Xu, J. Y.; Zhang, D. Z.; Chang, S. H.; Ho, S. T.; Seelig, E. W.; Liu, X.; Chang, R. P. H. *Phys. Rev. Lett.* **2000**, *84*, 5584.
(2) Bagnall, D. M.; Chen, Y. F.; Zhu, Z.; Yao, T.; Koyama, S.; Shen, M. Y.; Goto, T. *Appl. Phys. Lett.* **1997**, *70*, 2230.
(3) Service, R. F. *Science* **1997**, *276*, 895.
(4) Liu, C. H.; Zapien, J. A.; Yao, Y.; Meng, X. M.; Lee, C. S.; Fan, S. S.; Lifshitz, Y.; Lee, S. T. *Adv. Mater.* **2003**, *15*, 838.
(5) Shibata, T.; Unno, K.; Makino, E.; Ito, Y.; Shimada, S. *Sens. Actuators, A* **2002**, *102*, 106.
(6) Minne, S. C.; Manalis, S. R.; Quate, C. F. *Appl. Phys. Lett.* **1995**, *67*, 3918.
(7) Baratto, C.; Sberveglieri, G.; Onischuk, A.; Caruso, B.; Stasio, S. D. *Sens. Actuators, B* **2004**, *100*, 261.
(8) Nanto, H.; Minami, T.; Takata, S. *J. Appl. Phys.* **1986**, *60*, 482.
(9) Mitzner, K. D.; Sternhagen, J.; Galipeau, D. W. *Sens. Actuators, B* **2003**, *93*, 92.
(10) Sberveglieri, G.; Groppelli, S.; Nelli, P.; Tintinelli, A.; Giunta, G. *Sens. Actuators, B* **1995**, *24*−*25*, 588.
(11) Rao, G. S. T.; Rao, D. T. *Sens. Actuators, B* **1999**, *55*, 166.
(12) Yumoto, H.; Inoue, T.; Li, S. J.; Sako, T.; Nishiyama, K. *Thin Solid Films* **1999**, *345*, 38.
(13) Keis, K.; Vayssieres, L.; Lindquist, S. E.; Hagfeldt, A. *Nanostruct. Mater.* **1999**, *12*, 487.
(14) Hara, K.; Horiguchi, T.; Kinoshita, T.; Sayama, K.; Sugihara, H.; Arakawa, H. *Sol. Energy Mater. Sol. Cells* **2000**, *64*, 115.
(15) Zhu, Y. W.; Zhang, H. Z.; Sun, X. C.; Feng, S. Q.; Xu, J.; Zhao, Q.; Xiang, B.; Wang, R. M.; Yu, D. P. *Appl. Phys. Lett.* **2003**, *83*, 144.
(16) Huang, M. H.; Mao, S.; Feick, H.; Yan, H. Q.; Wu, Y. Y.; Kind, H.; Weber, E.; Russo, R.; Yang, P. D. *Science* **2001**, *292*, 1897.
(17) Lyu, S. C.; Zhang, Y.; Ruh, H.; Lee, H. J.; Shim, H. W.; Suh, E. K.; Lee, C. J. *Chem. Phys. Lett.* **2002**, *363*, 134.
(18) Zheng, M. J.; Zhang, L. D.; Li, G. H.; Shen, W. Z. *Chem. Phys. Lett.* **2002**, *363*, 123.
(19) Zhang, J.; Sun, L. D.; Pan, H. Y.; Liao, C. S.; Yan, C. H. *New J. Chem.* **2002**, *26*, 33.
(20) Pan, Z. W.; Dai, Z. R.; Wang, Z. L. *Science* **2001**, *291*, 1947.
(21) Ding, Y.; Gao, P. X.; Wang, Z. L. *J. Am. Chem. Soc.* **2004**, *126*, 2066.
(22) Yao, B. D.; Chan, Y. F.; Wang, N. *Appl. Phys. Lett.* **2002**, *81*, 757.
(23) Li, Y. B.; Bando, Y.; Sato, T.; Kurashima, K. *Appl. Phys. Lett.* **2002**, *81*, 144.
(24) Wang, X. D.; Summers, C. J.; Wang, Z. L. *Nano Lett.* **2004**, *4*, 423.
(25) Park, W. I.; Kim, D. H.; Jung, S. W.; Yi, G. C. *Appl. Phys. Lett.* **2002**, *80*, 4232.
(26) Wu, J. J.; Liu, S. C. *Adv. Mater.* **2002**, *14*, 215.
(27) Greene, L. E.; Law, M.; Goldberger, J.; Kim, F.; Johnson, J. C.; Zhang, Y. F.; Saykally, R. J.; Yang, P. D. *Angew. Chem., Int. Ed.* **2003**, *42*, 3031.
(28) Vayssieres, L.; Keis, K.; Lindquist, S. E.; Hagfeldt, A. *J. Phys. Chem. B* **2001**, *105*, 3350.
(29) Guo, L.; Ji, Y. L.; Xu, H. B. *J. Am. Chem. Soc.* **2002**, *124*, 14864.
(30) Liu, B.; Zeng, H. C. *J. Am. Chem. Soc.* **2003**, *125*, 4430.
(31) Vayssieres, L.; Keis, K.; Hagfeldt, A.; Lindquist, S. E. *Chem. Mater.* **2001**, *13*, 4395.
(32) Hu, J. Q.; Li, Q.; Meng, X. M.; Lee, C. S.; Lee, S. T. *Chem. Mater.* **2003**, *15*, 305.
(33) Lao, J. Y.; Wen, J. G.; Ren, Z. F. *Nano Lett.* **2002**, *2*, 1287.
(34) Park, W. I.; Yi, G. C.; Kim, M.; Pennycook, S. J. *Adv. Mater.* **2003**, *15*, 526.
(35) Tian, Z. R.; Voigt, J. A.; Liu, J.; Mckenzie, B.; Mcdermott, M. J. *J. Am. Chem. Soc.* **2002**, *124*, 12954.
(36) Dai, Y.; Zhang, Y.; Li, Q. K.; Nan, C. W. *Chem. Phys. Lett.* **2002**, *358*, 83.
(37) Yu, H. D.; Zhang, Z. P.; Han, M. Y.; Hao, X. T.; Zhu, F. R. *J. Am. Chem. Soc.* **2005**, *127*, 2378.
(38) Wang, S. H.; Yang, S. H. *Chem. Mater.* **2001**, *13*, 4794.
(39) Wen, X. G.; Zhang, W. X.; Yang, S. H.; Dai, Z. R.; Wang, Z. L. *Nano Lett.* **2002**, *2*, 1397.
(40) Zhang, W. X.; Wen, X. G.; Yang, S. H.; Berta, Y.; Wang, Z. L. *Adv. Mater.* **2003**, *15*, 822.
(41) Wen, X. G.; Xie, Y. T.; Choi, C. L.; Wan, K. C.; Li, X. Y.; Yang, S. H. *Langmuir* **2005**, *21*, 4729.
(42) Wen, X. G.; Wang, S. H.; Ding, Y.; Wang, Z. L.; Yang, S. H. *J. Phys. Chem. B* **2005**, *109*, 215.
(43) Yang, Q.; Tang, K.; Zuo, J.; Qian, Y. *Appl. Phys. A* **2004**, *79*, 1847.
(44) Fan, H. J.; Scholz, R.; Kolb, F. M.; Zacharias, M. *Appl. Phys. Lett.* **2004**, *85*, 4142.
(45) Vanheusden, K.; Warren, W. L.; Seager, C. H.; Tallant, D. R.; Voigt, J. A.; Gnade, B. E. *J. Appl. Phys.* **1996**, *79*, 7983.
(46) Yu, S. F.; Yuen, C.; Lau, S. P.; Lee, H. W. *Appl. Phys. Lett.* **2004**, *84*, 3244.
(47) Xu, C. X.; Sun, X. W.; Yuen, C.; Chen, B. J.; Yu, S. F.; Dong, Z. L. *Appl. Phys. Lett.* **2005**, *86*, No. 011118.
(48) Sun, X W.; Yu, S. F.; Xu, C. X.; Yuen, C.; Chen, B. J.; Li, S. *Jpn. J. Appl. Phys.* **2003**, *42*, L1229.